

## Supplementary Information:

# Thermal degradation of $\text{CH}_3\text{NH}_3\text{PbI}_3$ perovskite into $\text{NH}_3$ and $\text{CH}_3\text{I}$ gases observed by coupled thermogravimetry - mass spectrometry analysis

Emilio J. Juarez-Perez, Zafer Hawash, Sonia R. Raga, Luis K. Ono and Yabing Qi\*

*Energy Materials and Surface Sciences Unit (EMSS), Okinawa Institute of Science and Technology Graduate University (OIST), 1919-1 Tancha, Kunigami-gun, Onna-son, Okinawa 904-0495, Japan.*

\*Corresponding author: Yabing Qi. E-Mail: Yabing.Qi@OIST.jp

## Experimental Section

### S.1. Synthesis of $\text{CH}_3\text{NH}_3\text{PbI}_3$ single crystals

$\text{CH}_3\text{NH}_3\text{PbI}_3$  single crystals were prepared by the inverse temperature crystallization method reported elsewhere.<sup>1</sup> Briefly, 1 M of  $\text{PbI}_2$  (Sigma Aldrich, 99%) and  $\text{CH}_3\text{NH}_3\text{I}$  (Dyesol Ltd.) were dissolved in gamma-Butyrolactone (GBL) at 60 °C under ambient conditions. Subsequently, 2.5 mL of filtered solution using 0.22  $\mu\text{m}$  pore size PTFE filter was transferred to a new 5 mL vial. The new vial was kept in an oil bath at temperature of 120 °C for 12 hours, which induced growth of  $\text{CH}_3\text{NH}_3\text{PbI}_3$  crystals.

### S.2. TG/DTA-MS measurements

Simultaneous thermal gravimetric (TG) and differential thermal analysis (DTA) (TG-DTA2000SE, Netzsch) data were recorded in the temperature range from 25 to 700 °C, at heating rates from 5 to 20 °C  $\text{min}^{-1}$  (Figure S7) for small monocrystalline samples of  $\text{CH}_3\text{NH}_3\text{PbI}_3$  and  $\text{CH}_3\text{NH}_3\text{I}$  polycrystalline powder in alumina crucibles and using He as carrier gas. During several trials, specifically using a slow heating scan rate, it was observed that eventually the small monocrystalline sample jumped out of the crucible and the TG trace showed a characteristic sudden mass loss step. This behavior was avoided by burying the sample in alumina powder (the same material as crucibles) as it can be seen in Figure S6d.

Released gases from the TG-DTA apparatus were fed directly into the mass spectrometer (MS) using a heated Quartz Inert Capillary (QIC) (HPR-20/QIC, Hiden Analytical Ltd.), passed through a quadrupole mass filter for mass analysis scanning sequentially from  $m/z = 1$  to 200, and detected with a Faraday cup. As the control experiment, commercially available  $\text{CH}_3\text{NH}_2$ ,  $\text{NH}_3$  and HI aqueous solutions, and reagent grade  $\text{CH}_3\text{I}$  solutions were vaporized and fed directly to the mass spectrometer and the corresponding fragmentation profiles were compared with the available NIST mass spectra database (see Figure S4).<sup>2</sup>

### S.3.a TG/DTA-MS measurements under light, moisture and oxygen conditions.

The TG-MS setup was modified to incorporate a quartz window on the top of the cylindrical vertical oven and a white light source carried by an optic fiber to simulate the illumination to the sample during the measurement, see Figure S9a. Such a light source provides  $\sim 0.78$  Sun of power at the end of the cylindrical oven (10 cm long) as measured by a certified Si diode cell. It is reasonable to expect that the middle position inside the oven where the sample is placed is irradiated by  $\sim 1$  Sun of light power. Admittedly, the results obtained here would not match exactly the case with 1 Sun illumination from a calibrated solar simulator. Nevertheless, with the modified setup we were able to get valuable insight regarding the impact of light irradiation (under various gas environment conditions) on the chemical stability of perovskite. Table S2 enumerates the different experimental conditions used during the measurements. The composition of the carrier gas (He and O<sub>2</sub>) is regulated by two mass flow meters mixing both gases. The final composition of this synthetic “air” gas is verified by the MS equipment. The moisture content in the gas stream for Experiments # 3 and 6 is introduced by a gas bubbler filled with water at room temperature (RT). The exact water content in the gas stream is also confirmed by the MS equipment, which gives the water content of 0.018 Kg/m<sup>3</sup> gas equivalent to 78% of relative humidity at 25 °C for conventional air.

Overall, the main difference observed when using an oxygen or water rich carrier gas during the TG-DTA/MS measurements is the TG trace during the high temperature interval time. All experiments running with such oxidant agents into the carrier gas, the PbI<sub>2</sub> is partially converted to lead oxide (Pb<sub>x</sub>O<sub>y</sub>) ashes, which remain after the measurement is finished (see Figure S9, panels b, c, e and f).

If the carrier gas is exclusively He as in Experiments # 1 (dark) and 4 (light), the second step corresponding to the PbI<sub>2</sub> sublimation reaches completion with 0% of remaining mass, see Figure 1a and Figure S9d, respectively. Such a difference is most likely a result of a substantially higher sublimation temperature for Pb<sub>x</sub>O<sub>y</sub> than that for PbI<sub>2</sub>. On the other hand, the common feature for all these experiments despite the different conditions used is that the gases released during thermal decomposition of CH<sub>3</sub>NH<sub>3</sub>PbI<sub>3</sub> above 300 °C are still ammonia and methyl iodide. Specifically, the 142 m/z peak signature for methyl iodide release can be clearly detected for all cases. Minor subtle differences in retention times, shape peaks, noise signals and higher background when compared with the first reported canonical experiment (dark and pure He gas stream) can be attributed to the dead-end space introduced by the quartz window accessory, illumination and different gas composition.

### S.3.b TG/DTA-MS measurements at low temperatures.

The detection of the CH<sub>3</sub>I release at low temperatures using our TG-DTA/MS setup is nontrivial because such a low release rate of CH<sub>3</sub>I will be below the detection limit if using the same measurement conditions as before. Therefore, we have performed a specifically designed additional measurement to obtain the experimental results. The results indeed confirm that the proposed decomposition pattern also takes place at low temperatures. In the additional experiment, instead of using a monotonically rising heating temperature slope (20 °C/ min), we have programmed a temperature profile that operates at low

temperatures with oscillating heating/cooling cycles. In this way, we can observe that the 127 and 142 m/z peaks follow unambiguously the low temperature profile programmed, see Figure S10. If we run the experiment raising and holding the temperature only at 80 °C, it would be extremely difficult to distinguish a methyl iodide formation peak based on the MS output noisy signal because the release rate at 80 °C can be even smaller than the detection limit of the instrument. Therefore, by using the oscillating temperature cycles we effectively increase the signal-to-noise ratio (similar to the lock-in technique), and can indeed observe the associated oscillating m/z peaks in phase. The response for this perturbing input temperature signal shows unambiguously the oscillating 127 and 142 m/z peak for CH<sub>3</sub>I. Also, to increase the response speed during the MS measurements, instead of tracking the full range of 1-200 amu that can cause the lagging time problem during sampling, we focused only on the specific amu at least demonstrating that methyl iodide is a released gas at low temperatures.

#### S.4 DFT calculations to determine molecular structures and chemical reaction paths

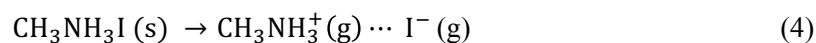
All DFT ground-state geometry optimizations, analytical frequency, thermodynamic variable states (studied between 25 - 600 °C temperature range at 1 atm of pressure) transition state and relaxed scan calculations for the molecular reactants, transition states and products species involved in reactions 3a and 3b were carried out using perturbatively corrected double hybrid functional with the Gershon Martin's "thermochemistry" reparametrization B2T-PLYP<sup>3,4</sup> as implemented in the ORCA 3.0.3 package.<sup>5</sup> Ground-state, transition state and relaxed scan calculations use minimally augmented diffuse and 0<sup>th</sup> order regular approximation (ZORA) recontracted scalar relativistic polarized triple zeta basis set (ma-ZORA-def2-TZVP) for all atoms.<sup>6-8</sup> In order to remove artificial overbinding effects from the basis set, a counterpoise correction gCP was carried out in states 2-4, 6 and 7 for the 3.a and 3.b chemical reaction path, respectively.<sup>9</sup> Energies for states 2-4 and 6 in Figure 2 of the main manuscript are reported with the applied gCP energy correction and Table S1 accounts numerically such energy correction applied for each state. Frequency calculations carried out at the same level of theory determined the nature of the stationary points for reactants and product characterized with zero imaginary frequency, except the transition state (state 3) for reaction 3.a. The only imaginary frequency found for state 3 is related to the breaking and forming bonds between iodine, methyl and ammonia fragments. Visualization of this imaginary frequency and relaxed scan optimizations were obtained using Gabedit.<sup>10</sup> Three short videofilms showing these relaxed scan calculations along the reaction coordinate and the imaginary frequency oscillation for state 3 have been deposited as support information.

#### S.5 Enthalpy of Crystallization Calculations

For the sake of completeness, we have also obtained the enthalpy of crystallization for CH<sub>3</sub>NH<sub>3</sub>I crystal phase and the enthalpy energy for one assemble of CH<sub>3</sub>NH<sub>3</sub><sup>+</sup> and I<sup>-</sup> ions in the pseudocubic structure of CH<sub>3</sub>NH<sub>3</sub>PbI<sub>3</sub> perovskite<sup>11</sup> to be compared with the enthalpy energy level of state 2 and 6 in Figure 2. To the best of our knowledge, the atomic position coordinates for the unit cell of CH<sub>3</sub>NH<sub>3</sub>I has not been reported. A PDF card entry in the ICDD database for CH<sub>3</sub>NH<sub>3</sub>I (no. 00-010-0737) exists and it indicates a tetragonal crystal lattice with unit cell parameters a = b = 5.12 Å and c = 9.00 Å for the title compound. We have carried out an *ab initio* structure determination of CH<sub>3</sub>NH<sub>3</sub>I from laboratory (Cu) powder X-Ray diffraction data to determine the heavy atom positions followed by a solid-state DFT/planewaves calculation to localize

the H atoms in the crystal structure. Our indexation process found plausible the orthorhombic group P 2 21 (a = 9.0225 Å, b = 5.1341 Å and c = 5.0958 Å) as space group. After that, the heavy atoms positions were located applying reciprocal space methods, simulated annealing and Rietveld refinement as implemented in the EXPO2014 toolkit software.<sup>12</sup> The ion pair interaction between CH<sub>3</sub>NH<sub>3</sub><sup>+</sup> and I<sup>-</sup> in the crystal structure shows a disposition of the three heavy atoms interacting in-line along the same axis, essentially as state 2 interaction calculated for gas phase (in contrast with state 6). The C-N bond distance obtained after Rietveld refinement is 1.481 Å. A CIF file text format can be found at end of this support information containing the obtained crystal structure for CH<sub>3</sub>NH<sub>3</sub>I. The H atom position for methylammonium was finally refined by geometry optimization using energy minimization in the solid state with the DFT/plane-waves approach using the PBE96 exchange-correlation functional as implemented in the NwChem 6.5 program.<sup>13</sup>

The hypothetical reaction equation dealing with the process fusion and evaporation of the solid state crystal phase can be described as:



where the left side of eq. 4 represents the ions assemble from our *ab initio* crystal structure determination of CH<sub>3</sub>NH<sub>3</sub>I and the right side of eq. 4 would be the interacting gas phase ion pair, the state 2 or state 6 geometry as obtained and depicted in Figure 2. Energy evaluation of both sides is carried out using the NwChem program using the same settings as the above H atom geometry optimization but without zero point, relativistic, thermal and vibration energy corrections. Similarly, the experimentally reported crystal structure for pseudo-cubic CH<sub>3</sub>NH<sub>3</sub>PbI<sub>3</sub> perovskite but stripped of one Pb<sup>2+</sup> and two I<sup>-</sup> ion is used as the ideal ions assemble representing formally a unit of CH<sub>3</sub>NH<sub>3</sub>I in the perovskite structure. Also, the H atom positions for methylammonium ion in the perovskite structure were refined using a DFT/planewave approach. Figure S8 shows the energy levels calculated for these solid state forms over imposed on the original Figure 2.

Figure S8 shows that the energy level calculated for the extended CH<sub>3</sub>NH<sub>3</sub>I (s) phase resembles the energy level for the ionic molecular pair interacting with state 2 geometry. It can be clearly understood because both set contain the same kind of interactions between the iodine ion and the methyl group in the methylammonium ion. On the other hand, the pseudocubic structure of perovskite contains two different sites for the iodine negative ion. It means that it is possible to build two different rearrangements for the CH<sub>3</sub>NH<sub>3</sub><sup>+</sup> and I<sup>-</sup> ions in perovskite disposition. Consequently, two energy levels can be calculated from this structure stripping off all Pb<sup>2+</sup> ions and leaving only one type of iodine. The two energy levels resembles the energy level for the ionic molecular pair interacting with state 6 geometry. Again, it can be clearly assimilated because both set contain the same kind of interactions between the iodine ion and the acidic hydrogen atoms in the -NH<sub>3</sub> group in the methylammonium ion. Globally, it means that any CH<sub>3</sub>NH<sub>3</sub><sup>+</sup> ⋯ I<sup>-</sup> interacting pair in the perovskite structure is more stable than the interacting pair in the CH<sub>3</sub>NH<sub>3</sub>I(s) crystal structure. Experimentally, it can be observed by a lower onset temperature of evaporation for CH<sub>3</sub>NH<sub>3</sub>I than a formal CH<sub>3</sub>NH<sub>3</sub>I ion pair in the CH<sub>3</sub>NH<sub>3</sub>PbI<sub>3</sub> perovskite structure.

## Supplementary Figures

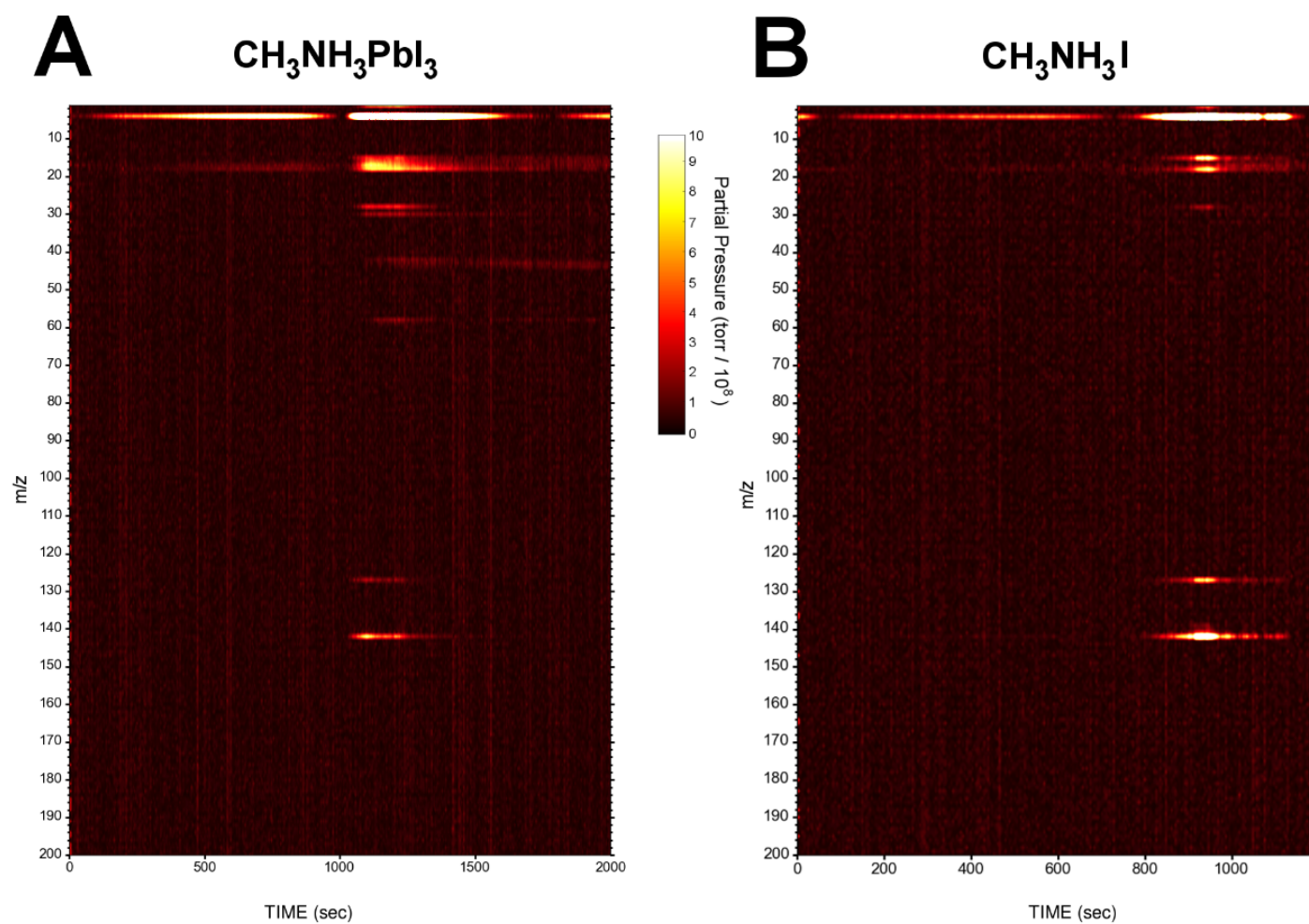


Figure S1. Full m/z (1 to 200 amu) vs. time contour plots recorded simultaneously in the MS equipment during the thermal degradation (heating rate of 20 °C/min) of a)  $\text{CH}_3\text{NH}_3\text{PbI}_3$  and b)  $\text{CH}_3\text{NH}_3\text{I}$ .

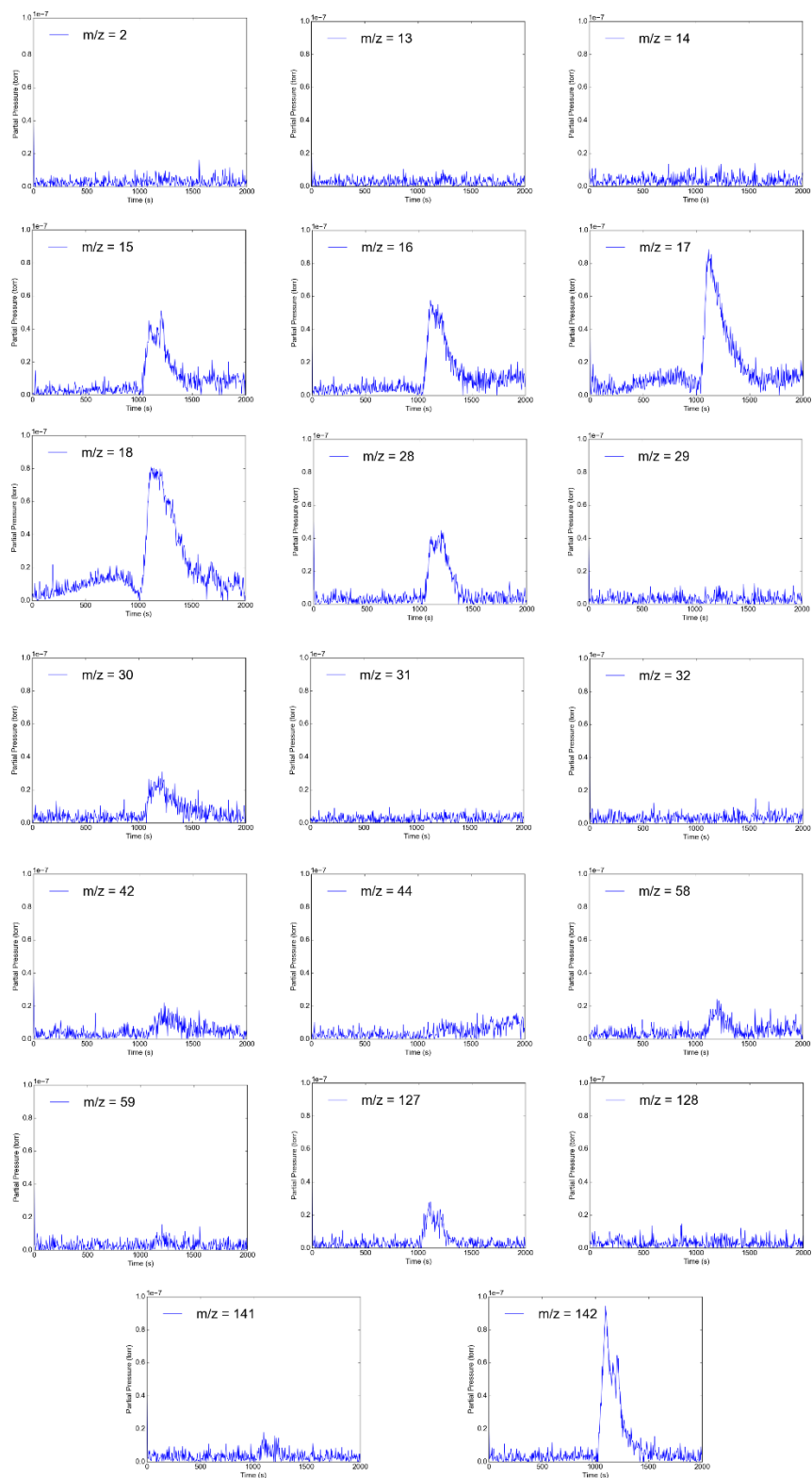


Figure S2. Partial pressure ( $10^{-8} - 10^{-7}$  torr) vs. time (0 – 2000 s) plots for selected m/z peaks recorded simultaneously in the MS equipment during the thermal degradation (heating rate of 20 °C/min) of  $\text{CH}_3\text{NH}_3\text{PbI}_3$ .

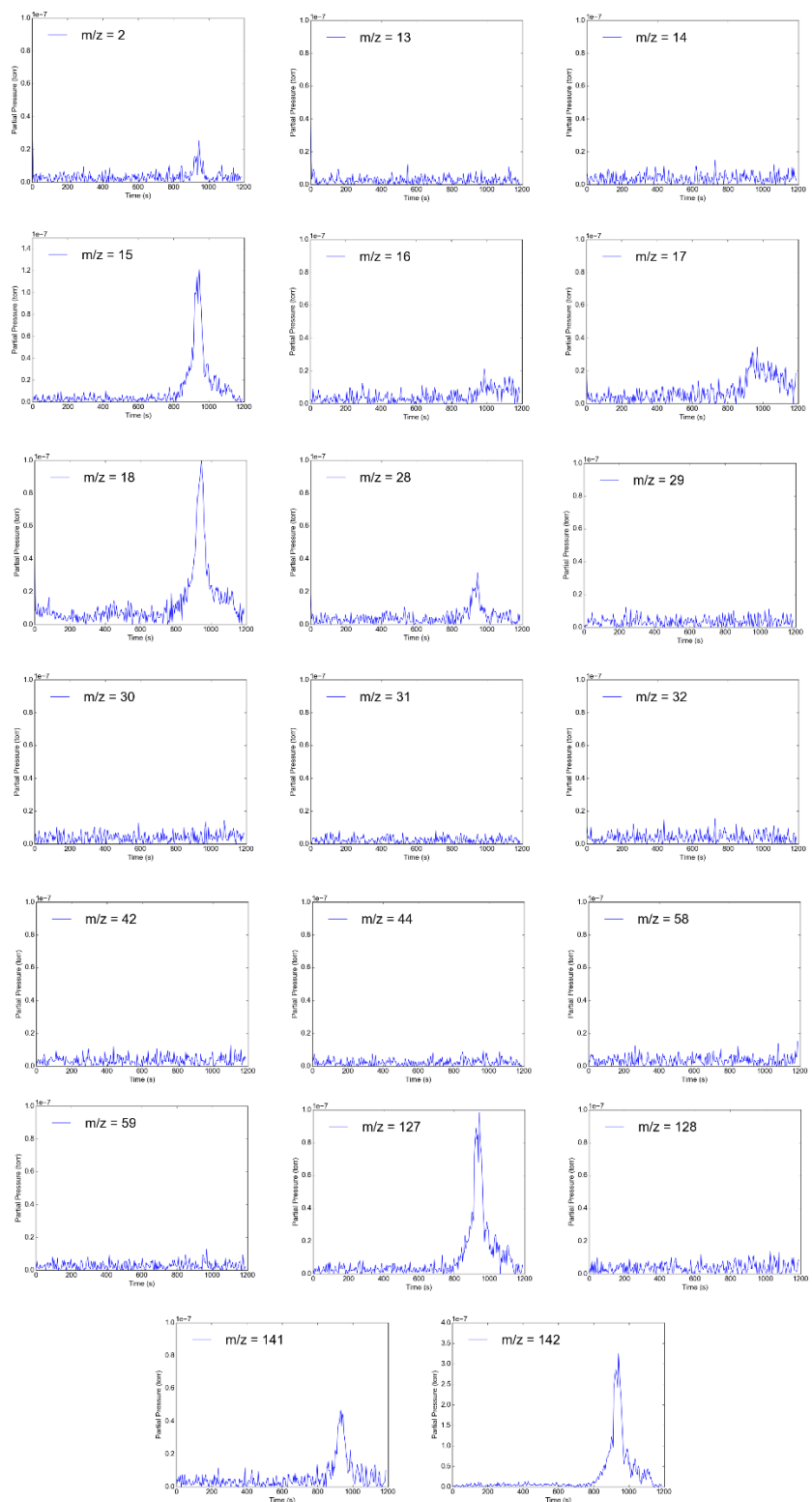


Figure S3. Partial pressure ( $10^{-8} - 10^{-7}$  torr) vs. time (0 – 1200 s) plots for selected  $m/z$  peaks recorded simultaneously in the MS equipment during the thermal degradation (heating rate of  $20\text{ }^{\circ}\text{C}/\text{min}$ ) of  $\text{CH}_3\text{NH}_3\text{I}$ .

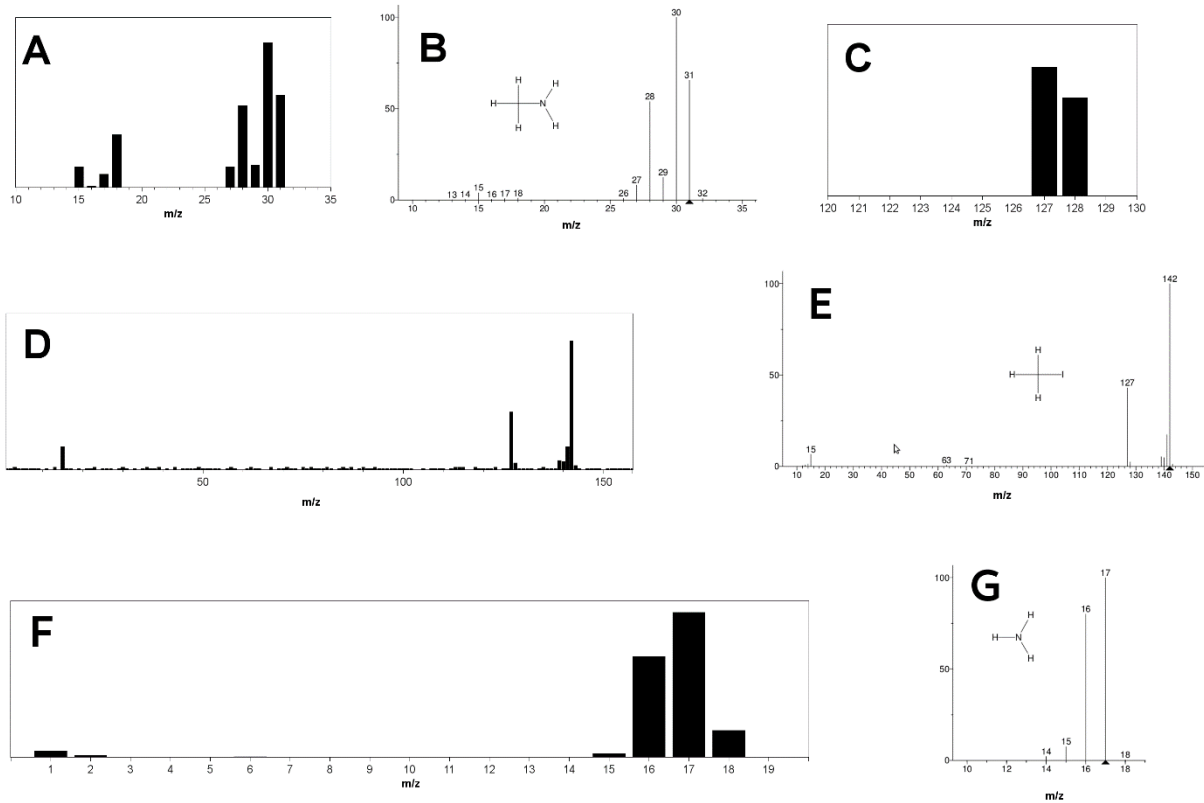


Figure S4. a) Experimental MS scan of 40 % (w/w) commercial methylamine water solution, b) methylamine mass spectrum from the NIST database<sup>2</sup>, c) Experimental MS scan of 40 % (w/w) commercial HI water solution, d) Experimental MS scan of methyl iodide, e) methyl iodide mass spectrum from the NIST database<sup>2</sup>, f) Experimental MS scan of 33% ammonia water solution e) NH<sub>3</sub> mass spectrum from the NIST database<sup>2</sup>.

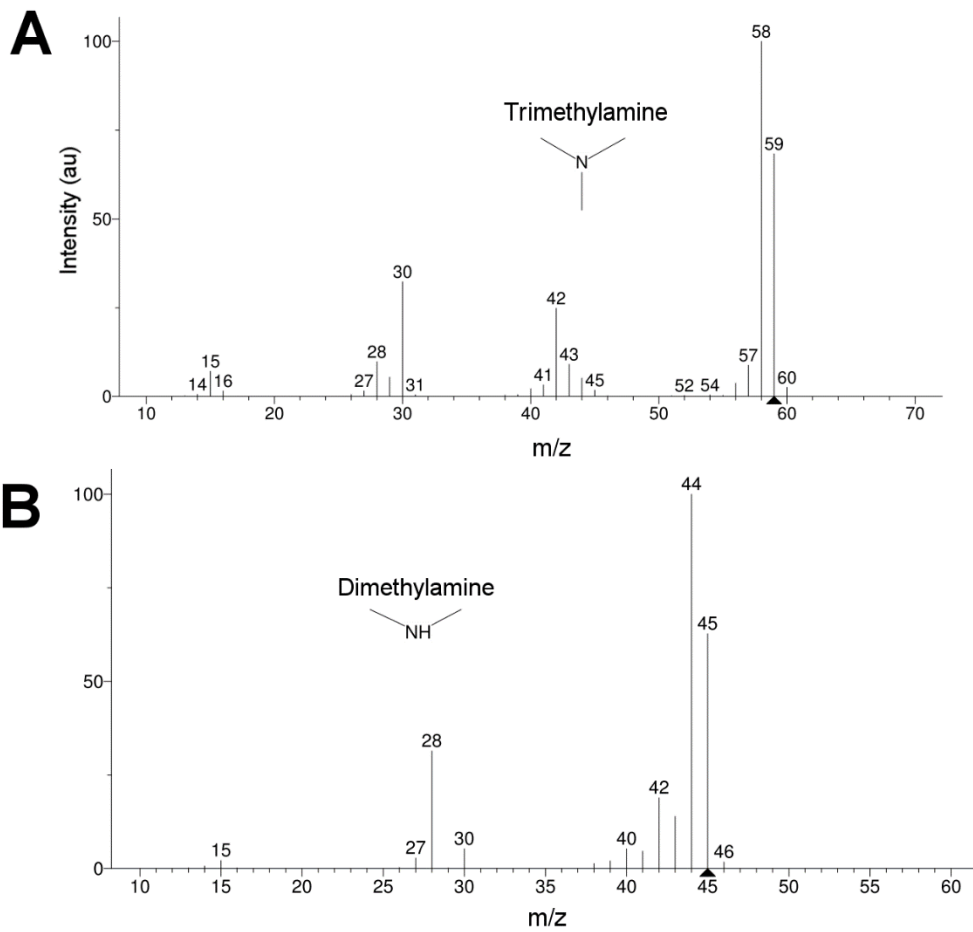


Figure S5. MS spectra from the NIST database<sup>2</sup> for a) trimethylamine and b) dimethylamine molecules.

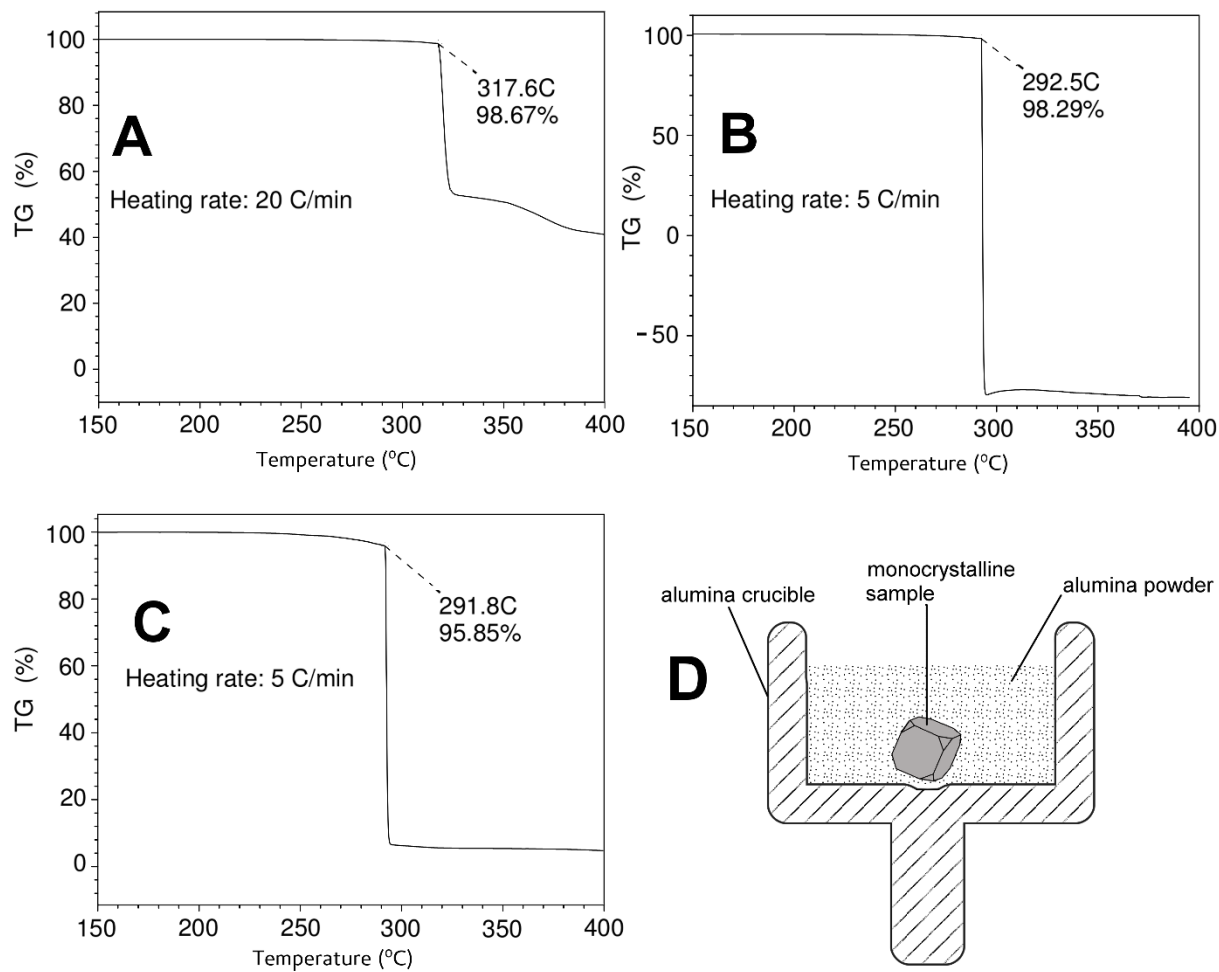


Figure S6. a-c) Examples of failed TG measurements because the monocrystal jumped out from the crucible during the temperature rise. d) Scheme depicting a perovskite monocrystal buried in alumina to avoid the jumping out during the TG measurement.

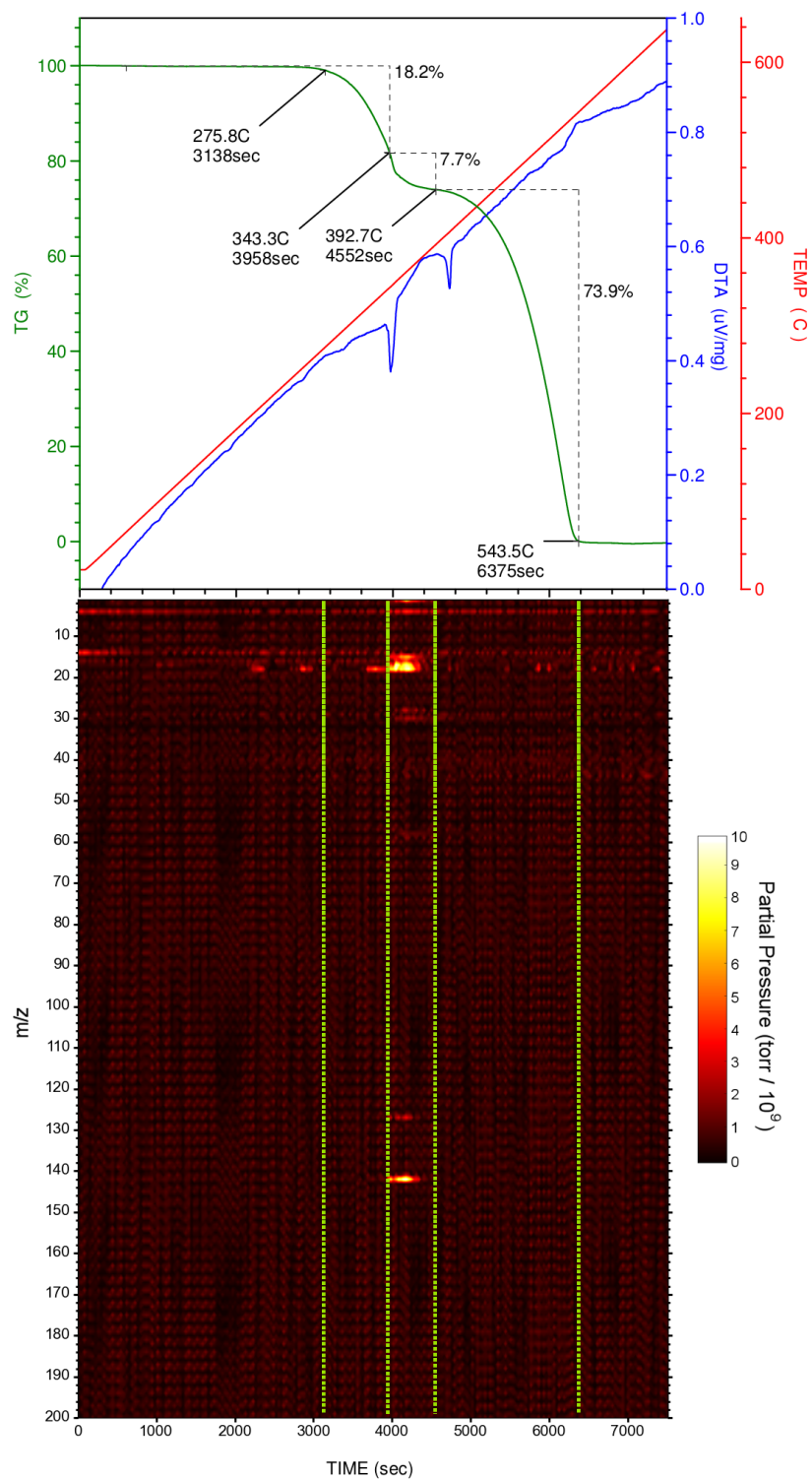


Figure S7. TG-DTA traces (upper panel, dark green and blue color trace, respectively.) and the  $m/z$  peaks recorded simultaneously during the thermal degradation (heating rate of  $5\text{ }^{\circ}\text{C}/\text{min}$ ) of  $\text{CH}_3\text{NH}_3\text{PbI}_3$ . Dashed green lines in the  $m/z$  vs time contour plots are guide to the eye delimiting the mass loss steps in the TG/DTA graph.

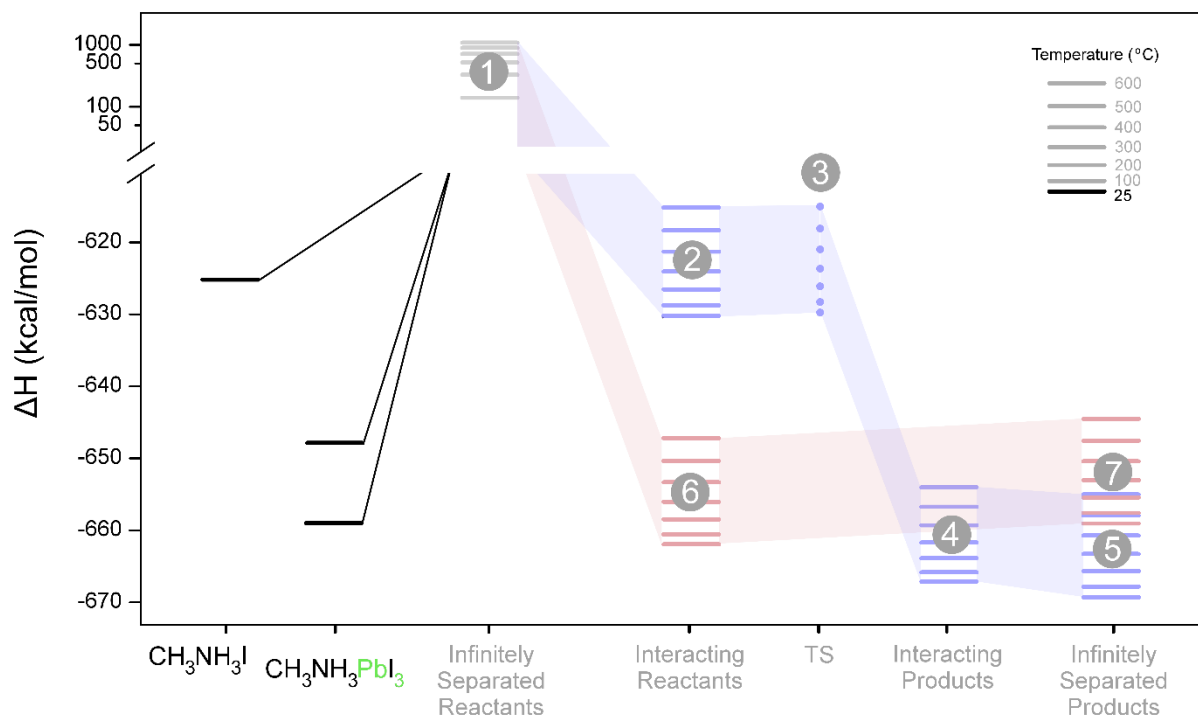


Figure S8. Thermodynamic cycle depicting the decomposition process from solid state  $\text{CH}_3\text{NH}_3\text{I}$  and the  $\text{CH}_3\text{NH}_3\text{I}$  ionic pair assemble in the pseudocubic structure of  $\text{CH}_3\text{NH}_3\text{PbI}_3$  perovskite. The blurred part of the graph corresponds to Figure 2 and it is depicted here for easy comparison of the energy levels obtained for solid state and gas phase components.

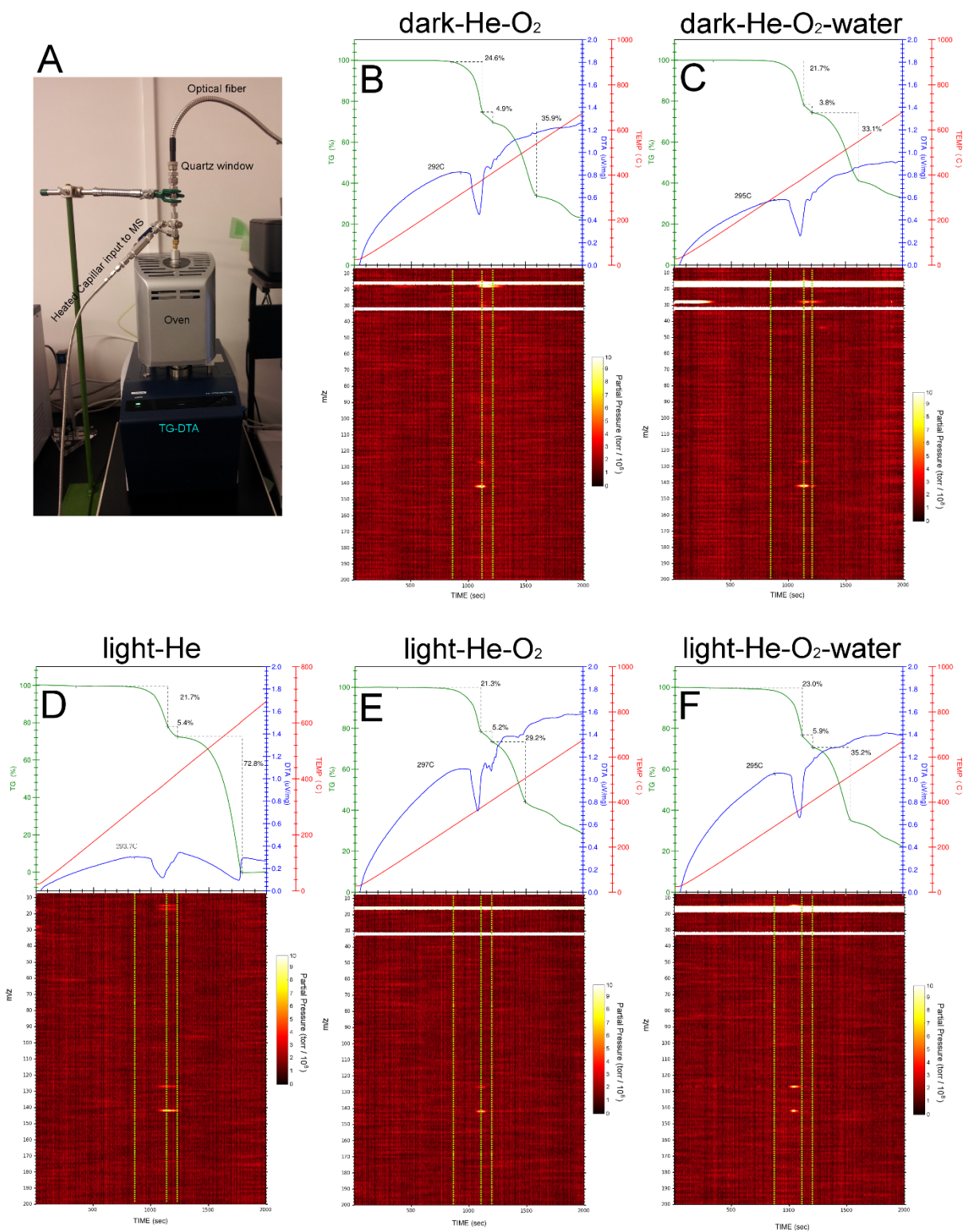


Figure S9. a) TG-DTA/MS equipment setup incorporating a quartz window and a light source. TG-DTA traces (upper panel, dark green and blue color trace, respectively.) and the m/z peaks recorded

simultaneously during the thermal degradation (heating rate of 20 °C/min) of  $\text{CH}_3\text{NH}_3\text{PbI}_3$  under b) dark using a dry gas mixture  $\text{He}/\text{O}_2$  (79/21 % v/v) as carrier gas, c) dark using a wet gas mixture  $\text{He}/\text{O}_2/\text{water}$  (77.5/21/2.5 % v/v) as carrier gas, d) light using a dry pure He gas as carrier gas, e) light using a dry gas mixture  $\text{He}/\text{O}_2$  (79/21 % v/v) as carrier gas, f) light using a wet gas mixture  $\text{He}/\text{O}_2/\text{water}$  (77.5/21/2.5 % v/v) as carrier gas.

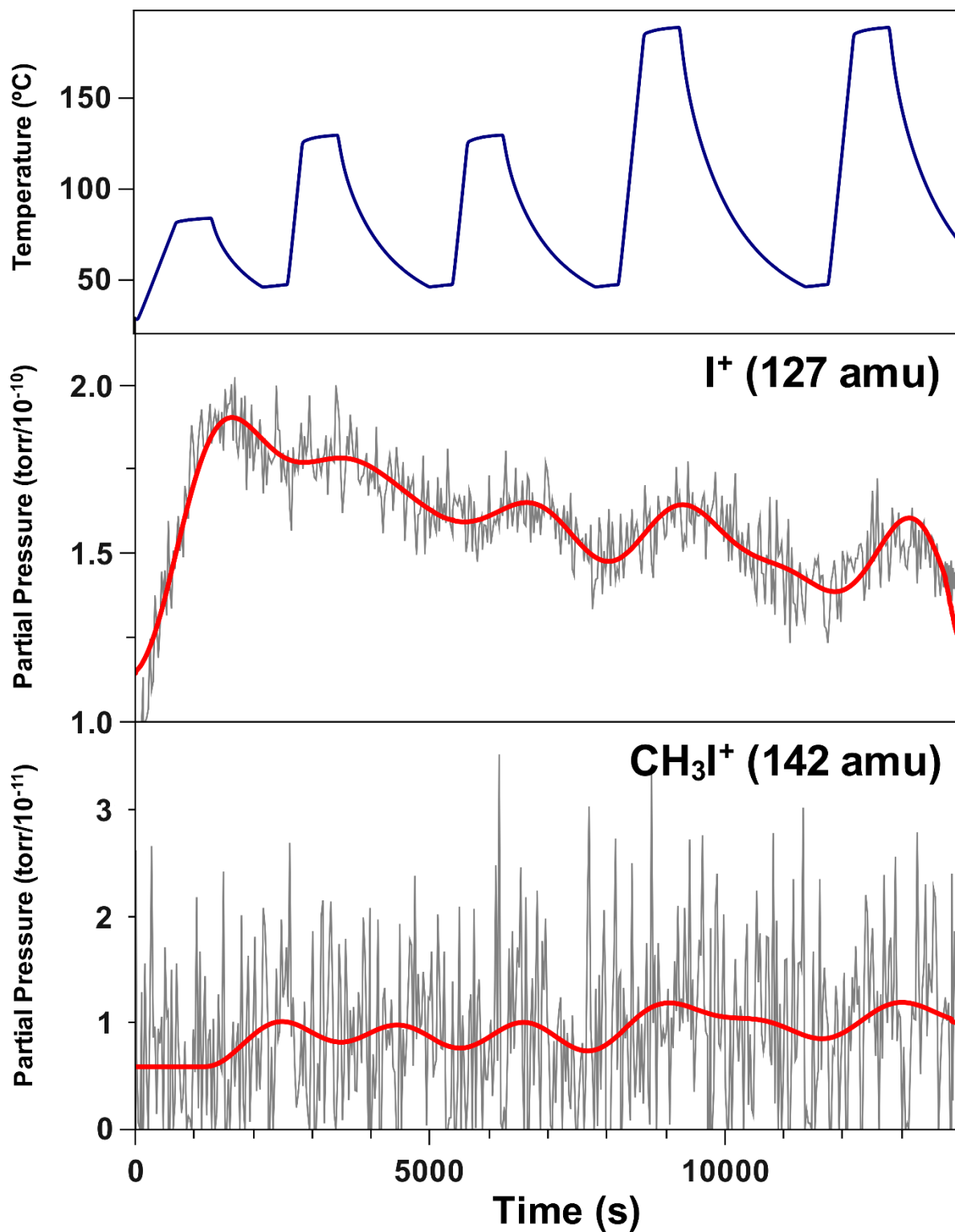


Figure S10. Upper panel is sample temperature recorded in the TG-DTA equipment. Middle panel is the recorded signal for the 127 amu peak. Lower panel is the recorded signal for the 142 amu peak. Raw data

from the MS detector without applying relative sensitivity factors and baseline corrections (gray trace) are smoothed using a FFT algorithm to help view (red trace).

## Supplementary Table

Table S1. Energy counterpoise correction gCP for states 2-4 and 6.

Interacting assemble	gCP correction (Hartree)
State 4	0.006702831
State 2	0.006873245
State 3	0.006886643
State 6	0.008032815

Table S.2 List of TG-MS experiments on perovskite degradation with the corresponding experimental conditions.

Experiment #	Release	Illumination	Carrier Gas	Moisture
1	Figure 1.a	Dark	He	No
2	Figure S.9b	Dark	He/O2 (79/21 % v/v)	No
3	Figure S.9c	Dark	He/O2/water (77.5/21/2.5 % v/v)	78%
4	Figure S.9d	Light	He	No
5	Figure S.9e	Light	He/O2 (79/21 % v/v)	No
6	Figure S.9f	Light	He/O2 (77.5/21/2.5 % v/v)	78%

## Appendix: CIF file for the crystal structure of CH<sub>3</sub>NH<sub>3</sub>I determined using powder X Ray.

```

_audit_creation_method      Expo2014
loop_
  _atom_type_symbol
  _atom_type_description
  _atom_type_scatter_source
  'C' 'Carbon' 'International Tables Vol C Tables 4.2.6.8 and 6.1.1.4'
  'N' 'Nitrogen' 'International Tables Vol C Tables 4.2.6.8 and 6.1.1.4'
  'I' 'Iodine' 'International Tables Vol C Tables 4.2.6.8 and 6.1.1.4'
  'H' 'Hydrogen' 'International Tables Vol C Tables 4.2.6.8 and 6.1.1.4'
_cell_length_a              9.02253
_cell_length_b              5.13411
_cell_length_c              5.09584
_cell_angle_alpha           90.000
_cell_angle_beta            90.000
_cell_angle_gamma           90.000
_cell_volume                 236.053
_diffraction_radiation_wavelength 1.540560
_diffraction_radiation_type 'Cu K\alpha-1~'
_symmetry_Int_Tables_number 18
_symmetry_cell_setting      orthorhombic
_symmetry_space_group_name_H-M 'P 2 21 21'
_symmetry_space_group_name_hall 'P 2bc 2'
loop_
  _symmetry_equiv_pos_site_id
  _symmetry_equiv_pos_as_xyz
  1 'x, y, z'
  2 'x, -y, -z'
  3 '-x, y+1/2, -z+1/2'
  4 '-x, -y+1/2, z+1/2'
loop_
  _atom_site_type_symbol
  _atom_site_label
  _atom_site_fract_x
  _atom_site_fract_y
  _atom_site_fract_z
  _atom_site_U_iso_or_equiv
  _atom_site_occupancy
  _atom_site_adp_type
I    I1    0.6894 0.0000 0.5000 0.0380 1.0000    Uiso
N    N1    0.2924 0.0000 0.5000 0.0380 1.0000    Uiso
C    C1    0.1282 0.0000 0.5000 0.0380 1.0000    Uiso
loop_
  _geom_bond_atom_site_label_1
  _geom_bond_atom_site_label_2
  _geom_bond_site_symmetry_1
  _geom_bond_site_symmetry_2
  _geom_bond_distance
N1 C1 . . 1.480679

```

## References

1. M. I. Saidaminov, A. L. Abdelhady, B. Murali, E. Alarousu, V. M. Burlakov, W. Peng, I. Dursun, L. Wang, Y. He, G. Maculan, A. Goriely, T. Wu, O. F. Mohammed and O. M. Bakr, *Nat Comms*, 2015, **6**, 7586.
2. S. E. Stein, "Mass Spectra" by NIST Mass Spec Data Center <http://webbook.nist.gov/chemistry/>
3. T. Schwabe and S. Grimme, *Physical Chemistry Chemical Physics*, 2007, **9**, 3397-3406.
4. S. Grimme, *The Journal of chemical physics*, 2006, **124**, 034108.
5. F. Neese, *Wiley Interdisciplinary Reviews: Computational Molecular Science*, 2012, **2**, 73-78.
6. J. Zheng, X. Xu and D. G. Truhlar, *Theoretical Chemistry Accounts*, 2011, **128**, 295-305.
7. D. A. Pantazis, X.-Y. Chen, C. R. Landis and F. Neese, *Journal of chemical theory and computation*, 2008, **4**, 908-919.
8. F. Weigend and R. Ahlrichs, *Physical Chemistry Chemical Physics*, 2005, **7**, 3297-3305.
9. H. Kruse and S. Grimme, *The Journal of chemical physics*, 2012, **136**, 154101.
10. A.-R. Allouche, *J. Comput. Chem.*, 2011, **32**, 174-182.
11. C. C. Stoumpos, C. D. Malliakas and M. G. Kanatzidis, *Inorg. Chem.*, 2013, **52**, 9019-9038.
12. A. Altomare, C. Cuocci, C. Giacovazzo, A. Moliterni, R. Rizzi, N. Corriero and A. Falcicchio, *Journal of Applied Crystallography*, 2013, **46**, 1231-1235.
13. M. Valiev, E. J. Bylaska, N. Govind, K. Kowalski, T. P. Straatsma, H. J. Van Dam, D. Wang, J. Nieplocha, E. Apra and T. L. Windus, *Computer Physics Communications*, 2010, **181**, 1477-1489.